VI International Conference on Computational Methods for Coupled Problems in Science and Engineering
COUPLED PROBLEMS 2015
B. Schrefler, E. Oñate and M. Papadrakakis(Eds)

HYGROTHERMAL BEHAVIOUR OF HEMP CONCRETE; EXPERIMENTAL EVIDENCES AND MODELLING

Antonin FABBRI*, Pierre-Antoine CHABRIAC*, Dac Thuong NGO*, Frederic SALLET*, Emmanuel GOURDON*, Henry WONG* and Jean-Claude MOREL*

*LGCB-LTDS, UMR 5513 CNRS, ENTPE
Universit de Lyon, F69100 Vaulx-en-Velin, France
e-mail: antonin.fabbri@entpe.fr, pierre-antoine.chabriac@entpe.fr, dacthuong.ngo@entpe.fr, frederic.sallet@entpe.fr, emmanuel.gourdon@entpe.fr, KwaiKwan.wong@entpe.fr, jean-claude.morel@entpe.fr

Key words: Instructions, Coupled Problems, Multiphysics Problems, Applications, Computing Methods

Abstract. This paper presents experimental hygrothermal data of an hemp concrete wall of dimensions $0.9 \times 0.9 \times 0.1$ [m^3]. The wall is instrumented with sensors to monitor temperature, relative humidity at the middle of the wall and incoming heat flows at the external surfaces. It is placed in a double climatic chamber that allows the regulation of temperature and relative humidity on each side of the wall, independently to each other. The experimental results leads to a clear identification of the coupling between the variation of the relative humidity inside the wall and its temperature. The validity of the commonly adopted assumptions for hygrothermal simulation are finally analyzed in the light of these experimental results. The material parameters used for the simulations are measured separately on decimetric samples of the same hemp concrete, which comes from the same mix and with the same apparent density.

1 INTRODUCTION

Buildings now represent 23.5% of the greenhouse gas emissions in France [1].This energy cost is due to buildings consumptions (heat, ventilation...), but also to the embodied energy required for their construction, their rheabilitation and their dismantling. In this context, the use of bio-based insulating materials like hemp concrete are gaining interest. Indeed, they allow to drastically reduce fossil energy consumption and greenhouse gas emissions associated with the manufacture compared to conventionally used materials for building insulation such as rock wool or fiberglass [2].
They are renewable, extracted from biomass and have promising thermal and acoustical

characteristics [3], [4], [5]. In addition, thanks to their ability to allow diffusion of water vapor within their porous network [6], these materials present an alternative option to isolate and rehabilitate buildings made with non-industrial materials (rammed earth, cob, adobe,...) and whose stability requires to maintain a water exchange with the outside [7]. The thermal conductivity of hemp concrete depends on its formulation, its implementation and its water content. It commonly ranges from 70 mW/(mK) to 300 mW/(mK) [8], which is quite high for an insulating material. In comparison, the thermal conductivities of expended polystyrene and glass wool are about 40 mW/(mK). However, the thermal performance of hygroscopic insulating systems like hemp concrete is commonly above that what can be expected by considering their sole characteristics on thermal conductance and their thickness. This higher performance can be attributed to the latent heat associated with the liquid-to-vapor phase change of the water contained in the porous network of the material.
Another impact of this in-pore water phase change is the moisture buffering abilities of these materials. For example, at building scale, it was shown that the use of hygroscopic materials leads to a significant reduction of moisture variation amplitudes, which thus induces energy saves on ventilation [9].
In this context, this paper focus on experimental identification and quantification of the couplings between the flows of heat and water mass within a hemp concrete wall of dimensions $0.9 \times 0.9 \times 0.1$ [m^3]. The tested material, the experimental device and the implementation of the wall are presented in a first section. Then, the results obtained for two kind of hygrothermal loadings are presented and discussed in the light of numerical simulations based on the system of equation developed by [10]. The test conditions are chosen in order to clearly observe the impact of hygrometry on temperature variations.

2 MATERIALS AND METHODS

2.1 Material

The binder used in this study is the Tradical PF70. It is mixed with water and hemp by the amounts indicated in Table 1. The mixture is then compacted in a framework of internal dimensions $0.9 \times 0.9 \times 0.11$ [m^3] by 8 successive layers.

Hemp/Binder kg/kg	water/Binder kg/kg	ρ_d kg/m^3	ϕ -	μ -	μ^e -	λ at $w = 0\%$ mW/(m.K)	λ at $w = 5\%$ mW/(m.K)
0,33	0,81	504	0.46	0.42	0.25	147	162

Table 1: Main characteristics of the tested material

In addition to the wall, the same batch is used to realize cylindrical samples of 16cm diameter and 32cm length and plates of dimensions $0.3 \times 0.3 \times 0.06$ [m^3]. These samples are used for porous, hydric and thermal characterizations. The wet density just after

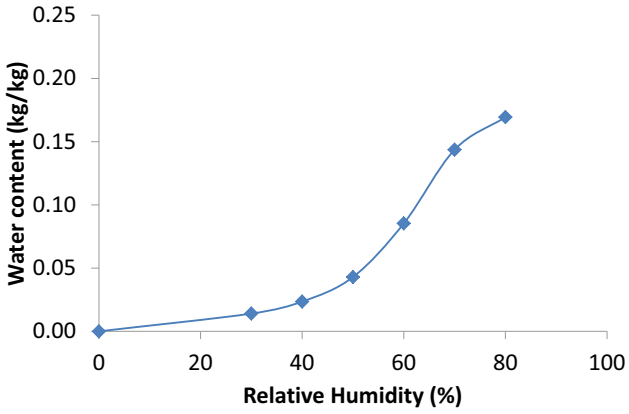

Figure 1: Sorption isotherm of the test hemp concrete at 20°C

the mixing of the wall, of the cylinders and of the plates are almost the same (800 $^{+}/_{-}$ 50 [kg/m^3]). The apparent dry density of the hemp concrete, ρ_d, is measured from the weighting of dried cylinders at 50°C, and the porosity, ϕ is estimated with a water pycnometer, through the relation : $\phi = (\rho_s - \rho_d)/\rho_s$, where ρ_s is the density of the skeleton estimated with the pycnometer.
The hydric characterization consists on a isothermal sorption isotherm following the NF EN ISO 12571 standard at 20°C , water vapor resistance (μ) following the NF EN ISO 12572 standard between relative humidities of 0% and 43.2%, and apparent water vapor resistance (μ^e) which is realized using the same protocol but at higher humidity (between 43.2% and 97%). These two last measurements allow to estimate the vapor and liquid transport characteristics, which are noted respectively δ_p and D_φ [10]:

$$\delta_p = \frac{\delta_a}{\mu} \; ; \; D_\varphi = p_{VS}\delta_a \left(\frac{1}{\mu^e} - \frac{1}{\mu} \right) \tag{1}$$

where δ_a is the vapor permeability of stagnant air (equal to 2.0 $\times 10^{-10}$ s at 20°C), and p_{VS} the saturated vapor pressure. This latter is an increasing function of temperature whose expression is well known and can be found, for example, in [11]. Let us underline that the value of D_φ obtained in this way remains valid only in the range of relative humidity used to estimate μ^e. A precise determination of this parameter would require the measurement of evolution of the relative permeability of the material with its water content.

Finally, the thermal conductivity, λ, is measured with a hot wire apparatus (Neotim - FP2C) and a hot plate apparatus (HFM - Netsch). The hot wire apparatus only allows

local measurements. Then, its accuracy is questionable when heterogeneous materials like hemp concrete are tested. To overcome this problem the thermal conductivities determined with this device are the average of a least five measurements at several locations of the sample. Using this protocol, the obtained result for the dried sample is similar to the one obtained with a standardized hot plate apparatus. In consequence, we can assume that the hot wire apparatus is suitable to estimate the thermal conductivity of the studied hemp concrete.
Thanks to its rapidity, the hot wire technique allows the determination of thermal conductivity of wet samples with a limited risk of water content variation during the measurement. The thermal conductivity of the tested material is then measured at both $w = 0\%$ and $w = 5\%$, where w is the gravimetric water content (defined as the mass of water within the pores per unit of solid skeleton mass). Hydric and thermal properties of the hemp concrete are reported in table 1 and in Figure 1 for the sorption curve. Let us underline that the obtained results are in the range of the values commonly observed in literature for this kind of material.

2.2 Calibration and design of the instrumentation scheme

The wall is instrumented with internal temperature and relative humidity sensors and with surface heat flow meters. It is placed in a double climatic chamber that allows the regulation of temperature and relative humidity on each side of the wall, independently to each other. The instrumentation of the wall is illustrated in Figure 2.
The accuracy of the temperature and heat measurements is first tested on a expended polystyrene wall whose thermal porperties are known and are equal to $\lambda = 40$ mW/(m.K) and $\rho C = 24$ kJ/(m^3.K). As illustrated in Figure 2, two temperature sensor are placed in the middle of the wall. The first one, called top-middle temperature sensor, is inserted from the top of the sample, while the other one, called side-middle temperature sensor, is inserted from the left side of the sample. The aim of these two measurements is to scan the impact of the temperature sensor implementation on the measurement accuracy.
For this preparatory test, the thermal solicitation consists in three steps. During the first one, the left climatic chamber temperature is held at 40°C and right climatic chamber temperature is held at 20°C. During the second stage, the temperature of both climatic chambers is fixed at 20°C. Finally, the last stage is the symmetric of the first one: the left climatic chamber temperature is kept at 20°C while the right climatic chamber temperature is increased to 40°C. Each stage lasts approximatively 4 hours.

The temperature and heat flow measurements are compared to a pure thermal one-dimensional calculation. The thermal equation, namely $\rho C \partial T/\partial t = \underline{\nabla} \cdot (\lambda \underline{\nabla T})$ where T is the absolut temperature in Kelvin and $\underline{\nabla}$ is the symbol Nabla, is solved with COMSOL Multiphysics using the PDE module. The simulation is made for a 1D geometry of length $L = 0.1$m (x direction). It represents the lateral section of the tested wall. The Fourier's boundary conditions are set according to the temperature measurement within climatic

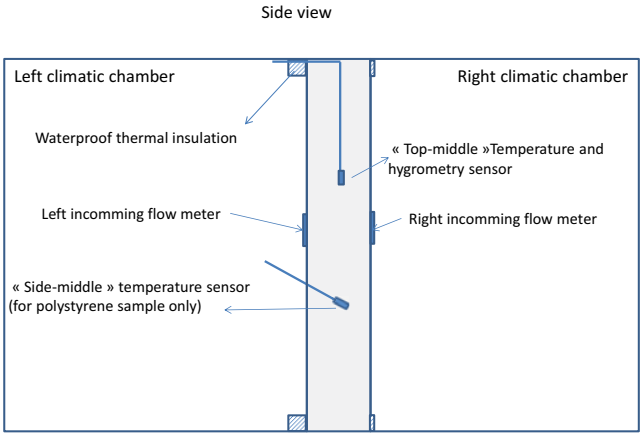

Figure 2: Schematic representation of the instrumentation of the wall

chambers and the heat transfer coefficients are supposed constant and respectively equal to 6 W/(m^2.K) for the left chamber and 7 W/(m^2.K) for the right one. These values are estimated from the average air velocity measurements within the climatic chambers at the vicinity of the wall which are equal to 0.1 m/s for the left one and 0.4 m/s for the right one.

Results, reported in Figure 3, show a good correlation between the measured and calculated incoming heat flows at both surface. The same conclusion can also be hold for the top-middle temperature sensor measurements. This comparison gives some confidence on the reliability of the temperature and heat flows which are measured. On the opposite, a significant difference is observed between the calculation and the measurements of the side-middle temperature sensor. Indeed, this latter remains very close to the temperature of the left climatic chamber, which suggest that, in that case, a significant thermal bridge is created between the sensor and the climatic chamber. In consequence, even if this experimental bias should be lowered when the thickness of the wall increases, the insertion of temperature sensor along the thermal gradient direction should be, whenever possible, avoided, and the measurement from temperature sensor instrumented in that way should be analyzed with care.

2.3 Definition of the loading paths

This paper focus on the coupling between heat and mass transfers within hemp concrete. To do so, two simple hygrothermal loadings are performed. The first one consists in a sudden increase of relative humidity within the two climatic chambers from 35% to

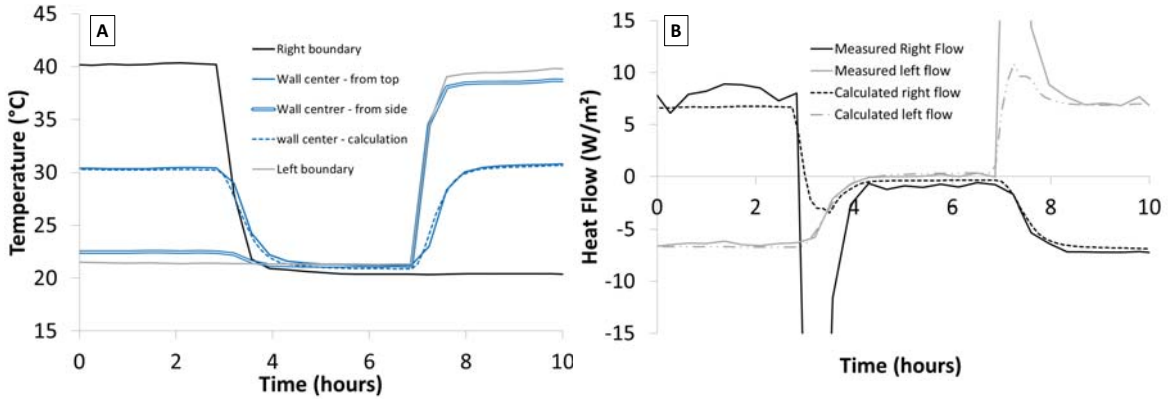

Figure 3: Comparison between the measured and the calculated temperature (A) and heat flows (B) for the polystyrene wall

80% at a constant temperature of 30°C. In that way, any variation of temperature in the middle of the wall and any heat flow across the wall surfaces would be induced by the condensation of water within the wall.
In the second experiment the left climatic chamber temperature is held at 30°C while the right one is held at 40°C. The two climatic chambers are initially at a relative humidity of 50%. After a stabilization period (that last about one week), a sudden increase of relative humidity from 50% to 80% is performed within both climatic chambers. Then, after another stabilisation period of 8 days, a sudden decrease of relative humidity from 80% to 50% is imposed within both climatic chambers. The purpose of this second experiment is to scan the effect of the phase change phenomena when the wall is submitted to temperature and vapor pressure differences between its two sides, and to compare the amplitude of the heat flow caused by this temperature difference and the one cause by the phase change processes. Let us underline that each loading are preceded by an equilibration period that last until the hygrometry and temperature measured within the wall are the same than the ones within the two climatic chambers.

3 RESULTS

The obtained variation of temperature and relative humidity within the two climatic chambers and at the middle of the wall during the first test are reported in Figure 4.

At first, even if the temperature within both climatic chambers remains fairly stable, the increase of relative humidity leads to a significant increase of temperature of 3°C within the wall. The shape of the wall temperature variation seems to follows the temporal derivation of the wall internal relative humidity (double-lined curve in Figure 4B).
The Figure 5A shows that this temperature increase go along with a decrease of the incoming heat flow at both sides down to significant negative values. Assuming that the

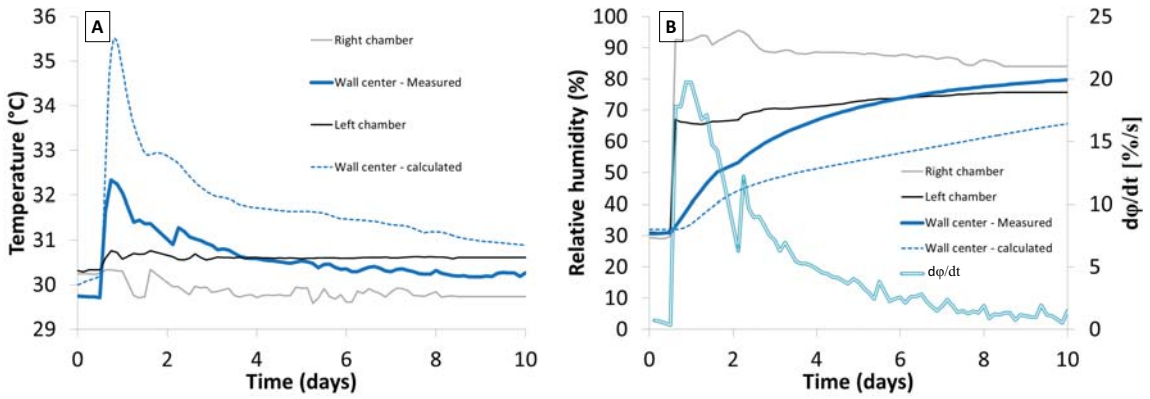

Figure 4: Temperature (A) and relative humidity (B) variations within the two climatic chamber and at the middle of the wall during the first test and their comparison with numerical results

heat flow through the isolated surfaces of the wall are negligible, the power provided by the wall due to the condensation process reads:

$$W = -(q_{left} + q_{right}) \tag{2}$$

where W is the supplied power per unit of wall lateral surface, while q_{left} and q_{right} are respectively the measured incoming heat flow through the left and right sides of the wall. It leads to values up to 10W/m^2. Given the fact that this supplied power remains higher than 6W/m^2 for at least 24 hours, the induced energy provided by the wall can become significant if an important surface of an hygroscopic wall is submitted to condensation.

Let us now observe the results from the second experiment which are reported in Figure 6 for the temperature and relative humidity variations and in Figure 5B for the heat flows. Similarly to the previous experiment, the wall temperature variation follows the same tendency than the variation of temporal derivation of relative humidity within the wall. An increase of the wall temperature (up to 1.5°C) is observed when the relative humidity increases and a decrease of wall temperature (down to 1.5°C) is observed when the wall relative humidity decreases. When the wall relative humidity returns to equilibrium with the relative humidity within the climatic chambers, no more phase change phenomena occurs and the temperature at the middle of the wall becomes equal to the average of the climatic chambers temperatures. In that case, the Figure 5B shows that the incoming heat flows from the left and right sides are opposite and equal to respectively -10W/m^2 and 10W/m^2. During the phase change processes, these two flows are no more directly opposite. The condensation process leads to a strong reduction of the incoming flow through the "hot" surface, while the evaporation process leads to a strong reduction of the outgoing flow though the "cold" surface. For at least 1 day, these reductions remain

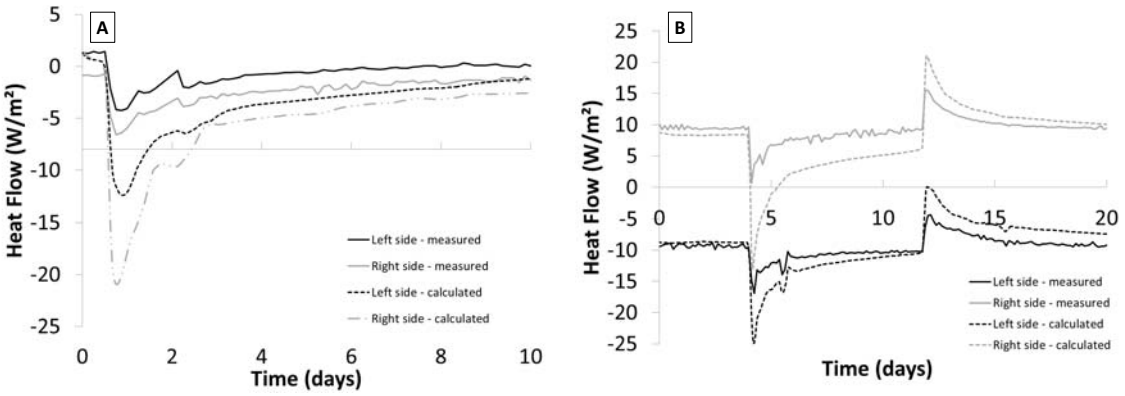

Figure 5: Heat flow at the left and right sides of the wall during the first (A) and the second (B) tests and their comparison with numerical results

higher than 75% of the heat flow induced by a temperature difference of 10°C between the chambers.

4 DISCUSSION

A simple way to explain the variation of temperature with time derivation of relative humidity is to consider the thermal equation in its unidimensional form for porous media with in-pore water phase change (proof reported in [12] and [11]):

$$\langle \rho C \rangle \frac{\partial T}{\partial t} = \underline{\nabla} \cdot (\langle \lambda \rangle \underline{\nabla T}) - L_V \overset{o}{m}_V \tag{3}$$

where L_V stands for the latent heat of evaporation/condensation, $\overset{o}{m}_V$ is the rate of water mass which evaporates per unit of material volume, $\langle \rho C \rangle$ is the average volumetric heat capacity of the material, and $\langle \lambda \rangle$ is its average thermal conductivity. These two latter vary with water content and temperature. However, only their variations with water content is considered here following the relations:

$$\langle \rho C \rangle = (1-\phi)\rho_s C_s + \rho_d w C_L + \left(\phi - \frac{w\rho_d}{\rho_L}\right) C_A \rho_A \ ; \ \langle \lambda \rangle = \lambda_0 + \delta_\lambda w \tag{4}$$

where $C_s = 1.6\text{kJ/(kg.K)}$ [13], $C_L = 4.2\text{kJ/(kg.K)}$ and $C_A = 1.0\text{kJ/(kg.K)}$ are the specific heat capacities of the solid skeleton, the liquid water and the wet air, while $\rho_A = 1\text{kg/m}^3$ and $\rho_L = 1000\text{kg/m}^3$ are the density of air and of liquid water. Finally, $\lambda_0 = 147\text{mW/(m.K)}$ is the dried thermal conductivity and $\delta_\lambda = 300\text{mW/(m.K)}$ is the variation of $\langle \lambda \rangle$ with water content. For illustration purpose, these two relations leads to $\langle \rho C \rangle = 981\text{kJ/(m}^3\text{.K)}$ and $\langle \lambda \rangle = 162\text{mW/(m.K)}$ at $w = 0.05$.

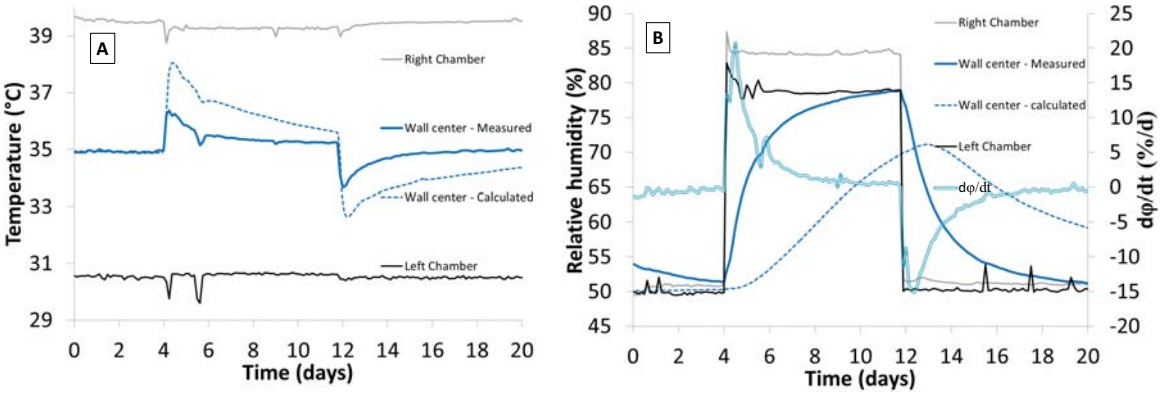

Figure 6: Temperature (A) and relative humidity (B) variations within the two climatic chamber and at the middle of the wall during the second test and their comparison with numerical results

According to the sorption curve of the material reported in Figure 1, the water content of the material increases with relative humidity. The obtained results are then consistent with eq. (3). Indeed, the relative humidity increases within the climatic chambers will lead to an increase of the water content of the wall and thus to condensation process within the porous network. In that case, $\overset{o}{m}_V$ is negative, and the last term of (3), which correspond to the heat supplied by the phase change process will be positive. On the opposite, a decrease of the chambers relative humidity leads to a positive $\overset{o}{m}_V$, and thus to heat consumption. However, the quantification of this effect is not so simple and a precise evaluation of $\overset{o}{m}_V$ requires a fully coupled hygrothermal model. To do so, it is commonly assumed that the equilibrium between the liquid water and its vapor is reach at anytime and anywhere within the porous network of the wall, and that the overall mass variation of water vapor can be neglected. Under these two assumptions, the mass conservation equation of water vapor leads to equality between the evaporation mass rate and the outgoing mass flow of vapor within the material :

$$\overset{o}{m}_V = -\underline{\nabla} \cdot \left(\delta_p \underline{\nabla \varphi p_{VS}}\right) \tag{5}$$

where φ is the relative humidity and p_{VS} is the saturated vapor pressure. Eq. (5) allows rewriting the thermal equation in the form :

$$\langle \rho C \rangle \frac{\partial T}{\partial t} = \underline{\nabla} \cdot \left(\langle \lambda \rangle \underline{\nabla T}\right) + L_V \underline{\nabla} \cdot \left(\delta_p \underline{\nabla \varphi p_{VS}}\right) \tag{6}$$

The outgoing mass flow of vapor within the material can eventually be estimated from the overall mass conservation of water. Assuming that the liquid water mass flow induced by temperature gradient at constant relative humidity is negligible and recalling that the water content is defined as $w = (m_V + m_L)/m_S$ where m_V, m_L and m_S are respectively

the mass of vapor, liquid water and solid skeleton, this latter reads:

$$\frac{\partial m_V + m_L}{\partial t} = \rho_d \frac{\partial w}{\partial t} = \underline{\nabla} \cdot \left(\delta_p \underline{\nabla \varphi p_{VS}} + D_\varphi \underline{\nabla \varphi} \right) \tag{7}$$

The system of equation (6)-(7), which was initially developed by [10], is the one which is commonly used to compute hygrothermal problems. It is solved with COMSOL Multiphysics using the PDE module. The simulations are made for a 1D geometry of length L=0.11m (x direction). It represents a cross section of the tested wall. Similarly to the purely thermal simulation realized on polystyrene, the Fourier's boundary conditions are set according to the measurement within the two climatic chambers and with heat exchange coefficients of 6 W/(m^2.K) for the left chamber and of 7 W/(m^2.K) for the right one. As suggested by [10] the moisture exchange coefficient is estimated to be equal to 25 10^{-9} kg/(m^2.s.Pa). No exchange of liquid water is assumed between the wall and the exterior. The material parameters used for the simulation are the ones reported in Table 1. Comparisons of calculated temperature, relative humidity and heat flows with their measurements are reported in Figures 4, 5 and 6.
Whatever the considered test, the system of equation (6)-(7) seems to overestimate the heat flows and the temperature variations while it tends to underestimate the variation of relative humidity at the middle of the sample. These two observation are contradictory. Indeed, to reach approximatively the same variation of the relative humidity, we need to consider a vapor resistance coefficient μ around 0.5 (which is, by the way, unrealistic since, by definition, μ should not be lower than 1). This decrease of μ will increase the vapor diffusion coefficient δ_p up to 4 10^{-10} kg/m/s/Pa and thus increase the heat source term, namely $L_V \underline{\nabla} \cdot \left(\delta_p \underline{\nabla \varphi p_{VS}} \right)$ in the thermal equation. In consequence, the difference between the calculated and measured heat flows and temperature would become even higher. To counterbalance this effect, we need to consider an specific thermal capacity C_d of about 150 000 J/(kg.K), which is clearly unrealistic and which leads to a significantly smoother temperature variation than the measured one.
In conclusion, the classical hygrothermal equation gives the good tendencies but does not seems to quantify correctly the hygrothermal behavior of the tested wall. Consequently, like it was recently made for raw earth materials by [11], the relevance of the simplifying assumptions which are commonly made in hygrothermal computations should be tested in the case of hemp concrete.

5 CONCLUSIONS

An hygrothermal experiment of an hemp concrete wall of dimensions $0.9 \times 0.9 \times 0.1$ [m^3] is presented. The wall is instrumented with sensors to monitor temperature, relative humidity at the middle of the wall and incoming heat flows at the external surfaces. It is placed in a double climatic chamber that allows the regulation of temperature and relative humidity on each side of the wall, independently to each other. Before the experiment, the accuracy of the measurement are tested on a calibrated material. This preliminary

test underlines the bias on temperature measurements when the sensors are introduced in the wall following the thermal gradient direction.
The test on the hemp concrete wall allows to observed its hygrothermal ability with a heat power supplied by the wall higher than 6W/m^2 during 24 hours when the relative humidity of the ambiance increase from 30% to 80%.
When a 10°C difference of temperature is imposed between the left and the right climatic chambers, the condensation process leads to a strong reduction of the incoming flow through the "hot" surface, while the evaporation process leads to a strong reduction of the outgoing flow though the "cold" surface. For at least 1 day, these reductions remain higher than 75% of the heat flow induced by a temperature difference of 10°C between the chambers.
Finally, the numerical computation of this experimental results underlines that the classical hygrothermal equation leads to the good tendencies, but does not seems to quantify correctly the behavior of the tested wall. The relevance of the simplifying assumptions which are commonly made in hygrothermal computations should thus be checked in the case of hemp concrete.

Acknowledgments : The present work is supported by the French Agency for Environment and energy Management (ADEME) through project IBIS (PIA - Projets d'Investissement d'Avenir).

REFERENCES

[1] Ministère de l'Ecologie, du Développement Durable et de l'Energie *Emissions de gaz à effet de serre (Monde, Europe, France)* (2013) URL http://www.developpement-durable.gouv.fr/Part-et-evolution-des-secteurs.htm.

[2] Harris, D. A quantitative approach to the assessment of the environmental impact of building materials. *Building and Environment* (1999) **34**:751–758.

[3] Pierre, T, Colinart, T, Glouannec, P. Measurment of thermal properties of biosourced building materials. *International Journal of Thermophysics* (2013).

[4] Asdrubali, F., Schiavoni, S., Horoshenkov, K.V. A review of sustainable materials for acoustic applications. *Build. Acoust.* (2013) **19**:283–312.

[5] Glé, P., Gourdon, E., Arnaud, L. Acoustical properties of materials made of vegetable particles with several scales of porosity. *Appl. Acoust.* (2011) **72**:249–259.

[6] Walker, R, Pavia, S. Moisture transfer and thermal properties of hemp-lime concretes. *Construction and Buildings Materials* (2014) **64**:270–276.

[7] Champiré, F, Fabbri, A, Morel, J-C and Wong, H. Experimental evidences of the atypical behavior of compacted earth materials. *Materials and Structures* (submitted).

[8] Collet, F, Pretot, S. Thermal conductivity of hemp concretes: variation with formulation, density and water content. *Construction and Buildings Materials* (2014) **65**:612–619.

[9] Woloszyn, M, Kalamees, T, Abadie, MO, Steeman, M, Sasic Kalagasidis A. The effect of combining a relative-humidity-sensituve ventilation system with the moisture buffering capacity of materials on indoor climate and energy efficiency of buildings. *Building and Environment* (2009) **44**:515–524.

[10] Künzel, M. *Simultaneous heat and moisture transport in building components one - and two-dimensional calculation using simple parameters* (1995) PhD thesis, Fraunhofer Institute of Building Physics.

[11] Soudani, L, Fabbri,A, Morel, J-C, Woloszyn, M, Chabriac, P-A, Wong, H, and Grillet, A-C. Experimental evidences of the atypical behavior of compacted earth materials. *Energy and Buildings* (In revision).

[12] Coussy, O. *Poromechanics* (2004) John Wiley & sons.

[13] Evrard, A. *Transient hygrothermal behaviour of Lime-Hemp Materials.* (2008) PhD thesis, Ecole polytechnique de Louvain, Belgique.